Fundamental Research 6 (2026) 2856–2868

Contents lists available at ScienceDirect

Fundamental Research

journal homepage: http://www.keaipublishing.com/en/journals/fundamental-research/

Article

Analysis of critical conditions for air bubble detachment from freezing fronts under different gravitational environments ☆

Keke Shao [a,b], Mengjie Song [a,*], Jun Shen [a], Dong Rip Kim [c], Xuan Zhang [a], Long Zhang [a], Zekang Zhen [a]

[a] Department of Energy and Power Engineering, School of Mechanical Engineering, Beijing Institute of Technology, Beijing 100081, China
[b] Department of Mechanical Engineering, The University of Tokyo, Tokyo 113-8654, Japan
[c] School of Mechanical Engineering, Hanyang University, Seoul 04763, South Korea

ARTICLE INFO

Article history:
Received 1 December 2024
Received in revised form 12 March 2025
Accepted 14 March 2025
Available online 3 April 2025

Keywords:
Air bubble
Detachment and trapping
Freezing front
Force analysis
Gravitational acceleration

ABSTRACT

Extraterrestrial water resources like water ice are essential for space activities. Exploration of ice formation processes in different gravitational environments will contribute to developing and utilizing these water ice resources. The formation of air bubbles on freezing fronts during icing is a common phenomenon, and their behavior of detachment or trapping directly affects ice properties. Mathematical modeling of the forces acting on air bubbles on freezing fronts is developed to investigate air bubbles' detachment and trapping conditions under different gravitational accelerations. The main forces affecting the state of bubbles are the lift force composed of buoyant, Marangoni, and thermomolecular forces, and the drag force composed of adhesion force and gravity. The equilibrium of the lift force and drag force is the critical mechanical condition for air bubble detachment and trapping, and the bubble radius at this time is defined as the critical detachment radius. The experimentally validated mathematical model predicts the air bubble detachment radius with an accuracy of > 65%, which is higher than the 30% of the existing model. The analysis reveals that among the forces affecting the bubble state, the Marangoni and adhesion forces are the dominant factors. The tilt angle of the freezing front, temperature gradient, and liquid density affect the bubble detachment radius, with the temperature gradient having the greatest effect. The study of the critical conditions for air bubble detachment and trapping under different gravitational environments can provide references for engineering applications such as space activities, metal casting, anti-icing, and deicing, as well as enrich the liquid-solid phase change mechanism.

1. Introduction

Bubbles are a very common substance that is found and used in many fields [1,2]. For example, boiling bubbles and cavitation bubbles are widely found in the energy sector [3,4]. The kinetic behavior of these bubbles can have a great impact on engineering applications and has been widely studied by scholars [5]. The behavior of boiling bubbles is affected by the surface, and when the voltage is changed, the nucleation and detachment behavior of the bubbles can be controlled [6]. In addition, the manipulation of bubble vesicle behavior using near-infrared light can be achieved by constructing a photopyroelectric slippery surface [7]. The discovery that surface tension is the determining factor in the rupture of bubbles in viscous liquids overturns the traditional belief that gravity is the determining factor [8]. The behavior of cavitation bubbles can also be described by having unified theoretical equations [9]. In addition, there is a class of air bubbles formed on freezing fronts during the freezing process, which has been less studied [10,11]. Especially, the kinetic study of air bubbles on freezing fronts is less involved [12,13]. Since these air bubbles can directly affect the physical properties of ice, which in turn affects engineering applications such as anti-deicing [14]. Therefore, an in-depth study of the kinetic behavior of air bubbles over freezing fronts is necessary.

The dissolution of air in water is a physical process that is different to avoid, 1g of water can dissolve up to 0.029g of air at 0 °C and one atmosphere. Since air has a much smaller solubility in ice, some air will be squeezed out of the ice and converge at the front of the freezing front during the icing process [15,16]. When the air concentration reaches a critical value, the supersaturated air nucleates to form tiny air bubbles [17,18]. These tiny air bubbles grow until they are covered by the freezing front to form trapped air bubbles or escape from the front to form detached air bubbles. Detached air bubbles account for 5%–60% of the total air bubble volume, up to half of the total number [19]. Trapped air bubbles have a significant effect on the physical properties of ice [20]. Not only does it reduce the mechanical strength and light transmission rate of the ice [21,22], but it also increases the thermal resistance to heat transfer [23]. Additionally, air bubbles in the ice can also serve

☆ Peer review under the responsibility of Editorial Board of Fundamental Research.

* Corresponding author.
E-mail address: mengjie.song@bit.edu.cn (M. Song).

https://doi.org/10.1016/j.fmre.2025.03.014
2667-3258/© 2025 The Authors. Publishing Services by Elsevier B.V. on behalf of KeAi Communications Co. Ltd. This is an open access article under the CC BY-NC-ND license (http://creativecommons.org/licenses/by-nc-nd/4.0/)

Nomenclatures

A	Hamaker constant
d	Water film thickness m
F_a	Adhesion force N
F_b	Buoyant force N
F_d	Drag force N
F_g	Gravity N
F_{Tm}	Thermomolecular force N
F_M	Marangoni force N
F_l	Lift force N
F_n	Normal force N
$F_{n,z}$	The z-component of the normal force N
F_t	Tangential force N
$F_{t,z}$	The z-component of the tangential force N
g	Gravitational acceleration m/s^2
k	Constant number
R	Radius m
s	Area m^2
t	Time s
T	Temperature K
x	Contact radius between the bubble and freezing front m

Greek symbols

β	Contact angle °
θ	Coordinate the angle in the yz plane. °
ρ	Density kg/m^3
σ	Surface tension N/m
φ	Coordinate the angle in the yz plane °

Subscripts

B	Bubble
c	Critical
cp	Cold plate
I	Ice
W	Water

as containers for storing gases such as hydrogen and ozone [24,25]. Therefore, studying the behavior of air bubbles on the freezing front will guide the preparation of clear ice bodies, the optimization of anti-icing and de-icing techniques, and even the exploitation of water ice resources in extraterrestrial galaxies.

The forces on air bubbles in freezing fronts have been analyzed by some scholars. Meano believes that air bubbles over freezing fronts are subjected to adhesion and buoyant forces [18]. Bagdasarov believes that the relative magnitude of buoyant force and capillary forces determines the state of air bubbles [26]. Cole suggests that buoyant, normal, and tangential forces comprise the lifting force driving air bubble detachment [27]. However, their model calculated that the radii of the air bubbles detached from the freezing front were all larger than the experimental values. This suggests that these models do not take into account all of the forces that affect air bubble detachment. A comparison of the values predicted by these models for the bubble detachment radius in the same situation is shown in Fig. 1, and it can be found that although all of their predicted values decrease with the increase of the contact angle, there are large differences between them. Moreover, there is a lack of experimental results for the validation of the models. Therefore, it is also necessary to carry out experimental and mathematical modeling studies on the critical conditions for bubble detachment and trapping over freezing fronts.

Gravity affects the efficiency of hydrogen production from electrolytic water by influencing the size of bubbles detached from the electrodes and thus the efficiency of hydrogen production from electrolytic water [28,29]. Gravity will therefore also have an effect on the detachment and trapping behavior of air bubbles on the freezing front during

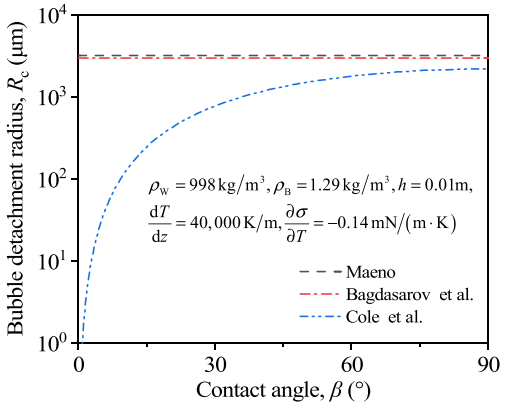

Fig. 1. Comparison of models predicting bubble detachment radius.

the freezing process. Trying to modulate the physical properties of ice by manipulating trapped air bubbles in ice requires an understanding of the critical mechanical conditions for the trapping and detachment of air bubbles on freezing fronts [30,31]. Gravitational acceleration affects the buoyant force acting on air bubbles and thus the state of the bubbles. The critical mechanical conditions for the detachment of air bubbles from freezing fronts in extreme gravitational environments have not been well studied [32]. Therefore, to pave the way for the experiment, the critical mechanical conditions of air bubble detachment and trapping under different gravitational environments will be analyzed by validated mathematical models.

To obtain the critical conditions for the air bubble trapping and detachment on the freezing front under different gravitational accelerations, a mathematical model describing the radius of air bubble detachment has been developed based on the principle of force equilibrium. The model defines the forces that drive the air bubbles to detach from the freezing front as lift forces, which include temperature gradient, thermomolecular and buoyant forces, and the forces that impede the detachment as drag forces, which include adhesion force and gravity. To verify the accuracy of the model, an experimental setup for freezing a pure water film in the vertical direction is constructed. Based on the validated model, the effects of the tilt angle of the freezing front, temperature gradient, and liquid density on the detachment radius of air bubbles and the force under different gravitational accelerations are further explored. In addition, the discussion range of gravitational acceleration is set from 0 to 100 m/s^2, taking into account the weightlessness and the maximum pressure that the human body can withstand, and the temperature gradient is set from 10 k/m to 10,000 k/m, taking into account the different heat transfer characteristics of different liquids. The study of critical conditions for air bubbles to detach from freezing fronts under different gravitational environments will not only provide references for the development and utilization of water ice resources in extreme environments and the development and optimization of anti-icing and de-icing technologies but also be expected to provide a research direction for metal smelting and the preparation of special ice.

2. Methodology

2.1. Modeling methodology

To analyze the critical conditions for the detachment of air bubbles from freezing fronts, a mathematical model based on the principle of hydrostatic equilibrium is carried out. The model takes full account of the forces on air bubbles over vertical and inclined freezing fronts at different gravitational accelerations. The morphology of an air bubble on a freezing front is shown in Fig. 2. To simplify the analysis without losing accuracy, the model is built with some assumptions that have been given in previous work [31,33]. The detachment of an air bubble

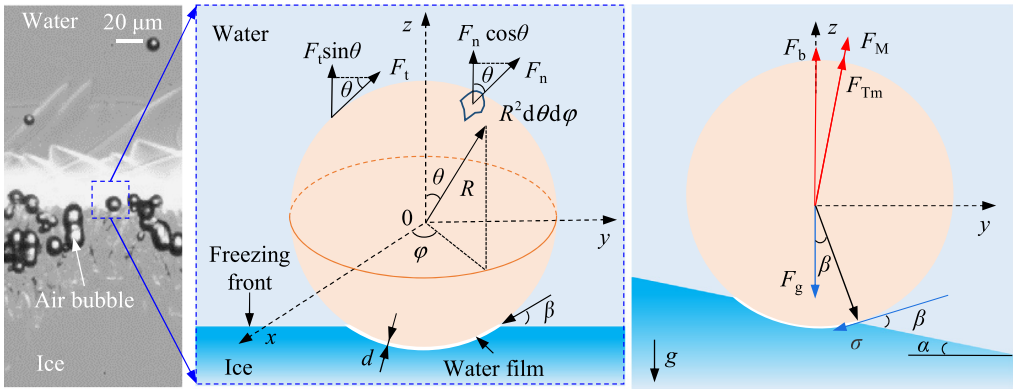

(a) Physical photo of air bubbles in ice **(b)** The shape of air bubble in water **(c)** Air bubble on inclined freezing front

Fig. 2. Schematic of the force acting on an air bubble.

from a freezing front is the result of the interaction of multiple forces acting on it (**Video-1**). In the vertical direction, the forces acting on the air bubble can be divided into the lift force that causes it to detach from the freezing front and the drag force that prevents it from detaching from the freezing front. The lift force is the resultant force of buoyant, thermomolecular force, and Marangoni force, while the drag force is the resultant force of adhesion and gravity. Before analyzing the forces on an air bubble, the shape of the bubble is first explored. The Bond number of the air bubble in the water is

$$\mathrm{Bo} = \frac{\rho_W g R^2}{\sigma} \tag{1}$$

where ρ_W is the density of the water, σ is surface tension, and R is the air bubble radius. The radius of the air bubble on the freezing front is 10^{-5} to 10^{-4} m, and the Bond number is 0.000000125 ~ 0.0000128. The Bond number is much < 1, indicating that the effect of gravity on the shape of the bubbles is negligible and that the bubbles on the freezing front remain spherical under surface tension.

(1) Lift force analysis

The buoyant force F_b acting on the bubble is equal to the gravitational force of its same volume of liquid, which can be expressed as [34]:

$$F_b = \frac{4}{3}\pi R^3 \rho_W g \tag{2}$$

Due to the Gibbs-Thomson effect, an ultrathin water film will exist between the air bubble and the freezing front [35,36]. Non-retarded Van der Waals interactions within ultrathin water film can be expressed as [37,38]

$$P_{Tm} = \frac{A}{6\pi d^3} \tag{3}$$

where A is the Hamaker constant, and d is the ultrathin water film thickness between the air bubble and the freezing front.

The thermomolecular force F_{Tm} exerted on the air bubble by this interaction within the ultrathin water film can be obtained by integration, which can be expressed as [39,40]

$$F_{Tm} = 2\pi R^2 \int_0^{\beta} \cos\beta \sin\beta P_{Tm} \mathrm{d}\beta \tag{4}$$

$$F_{Tm} = \frac{A R^2 \sin\beta}{6d^3} \tag{5}$$

The normal force acting on the air bubbles is composed of atmospheric pressure, hydrostatic pressure, and surface tension, which can be expressed as [27]

$$F_n = \left(P - \rho g R \cos\theta + \frac{2\sigma}{R}\right) R^2 \sin\theta \mathrm{d}\theta \mathrm{d}\varphi \tag{6}$$

To simplify the analysis, the air bubble on the freezing front is considered a sphere. The analysis shows that the force driving the air bubble to expand outward comes from the pressure difference between its inside and outside, which is mainly caused by the surface tension. The outward expansion force of the bubble caused by the pressure difference is called the normal force, which can be expressed as

$$F_n = \frac{2\sigma}{R} R^2 \sin\theta \mathrm{d}\theta \mathrm{d}\varphi \tag{7}$$

The combined normal force in the z-axis direction is

$$F_{n,z} = \int_0^{2\pi} \int_0^{\pi} \frac{2\sigma}{R} R^2 \sin\theta \cos\theta \mathrm{d}\theta \mathrm{d}\varphi \tag{8}$$

The pressure difference due to surface tension during the outward expansion of an air bubble is

$$\Delta P = \frac{\mathrm{d}\sigma}{R\mathrm{d}\theta} \tag{9}$$

The component of the tangential force F_t acting on a unit area $R^2\mathrm{d}\theta\mathrm{d}\varphi$ in the z-axis direction is

$$F_{t,z} = \frac{1}{R}\frac{\mathrm{d}\sigma}{\mathrm{d}\theta} R^2 \sin\theta \mathrm{d}\theta \mathrm{d}\varphi \tag{10}$$

The combined normal force in the z-axis direction is [27]

$$F_{t,z} = -\int_0^{2\pi} \int_0^{\pi} \frac{1}{R}\frac{\mathrm{d}\sigma}{\mathrm{d}\theta} R^2 \sin^2\theta \mathrm{d}\theta \mathrm{d}\varphi \tag{11}$$

where $(1/R)(\mathrm{d}\sigma/\mathrm{d}\theta)$ is the tangential component of the surface tension.

Assuming that the temperature distribution in the water near the freezing front has a liner distribution $\mathrm{d}T/\mathrm{d}z$, the temperature at any position of the air bubble can be related to the temperature gradient, direction angle, and contact angle as shown in Fig. 3. The temperature at the freezing front is T_f, then the temperature at any Point A on the air bubble can be expressed in the form of Eq. (12).

$$T = T_f + R(\cos\beta + \cos\theta)\frac{\mathrm{d}T}{\mathrm{d}z} \tag{12}$$

where T_f is the temperature of the freezing front and $\mathrm{d}T/\mathrm{d}z$ is the temperature gradient in water above the freezing front.

Surface tension can be expressed as

$$\sigma = \sigma_f + (T - T_f)\frac{\mathrm{d}\sigma}{\mathrm{d}z} \tag{13}$$

$$\sigma = \sigma_f + R(\cos\beta + \cos\theta)\frac{\mathrm{d}T}{\mathrm{d}z}\frac{\mathrm{d}\sigma}{\mathrm{d}T} \tag{14}$$

where σ is surface tension, σ_f is surface tension at temperature T_f.

Substituting Eq. (14) into Eqs. (7) and (11) yields

$$F_{n,z} = -\frac{8}{3}\pi R^2 \frac{\mathrm{d}T}{\mathrm{d}z}\frac{\mathrm{d}\sigma}{\mathrm{d}T} \tag{15}$$

$$F_{t,z} = -\frac{8}{3}\pi R^2 \frac{\mathrm{d}T}{\mathrm{d}z}\frac{\mathrm{d}\sigma}{\mathrm{d}T} \tag{16}$$

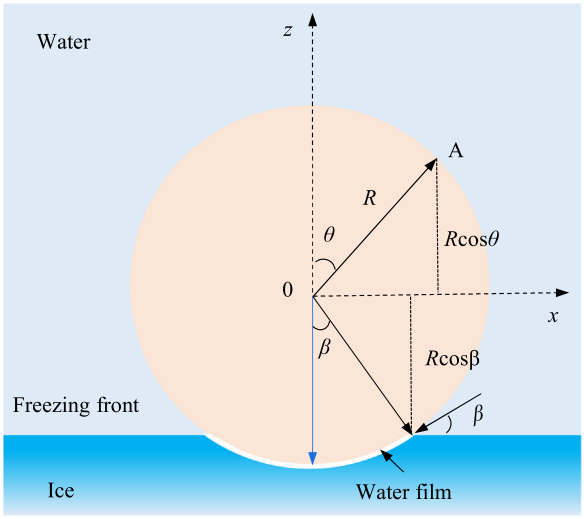

Fig. 3. Temperature distribution in the water in front of the freezing front.

The components of the normal and tangential forces in the z-axis direction have the same form, and they are essentially Marangoni forces due to temperature gradient, so they can be combined as Marangoni forces F_M.

$$F_M = -\frac{16}{3}\pi R^2 \frac{dT}{dz}\frac{d\sigma}{dT} \tag{17}$$

The lift force can be expressed as

$$F_l = F_b + F_{Tm} + F_M \tag{18}$$

(2) Drag force analysis

The adhesion force F_a that prevents the air bubble from detaching from the freezing front can be expressed as

$$F_a = 2\pi\sigma R\sin^2\beta \tag{19}$$

where β is the contact angle between the air bubble and the freezing front.

The gravity F_g can be expressed as

$$F_g = \frac{4}{3}\pi R^3 \rho_B g \tag{20}$$

where ρ_B is air bubble density.

The drag force acting on the air bubble is

$$F_d = F_a + F_g = 2\pi\sigma R\sin^2\beta + \frac{4}{3}\pi R^3\rho_g g \tag{21}$$

(3) Air bubble detachment radius

When the drag force acting on an air bubble is greater than the lift force, the bubble will cling firmly to the freezing front. When the lift force is greater than the drag force, the air bubble will detach from the freezing front. Therefore, equal lift and drag forces are the critical conditions for the air bubble to detach from the freezing front. The radius of the air bubble is called the air bubble detachment radius R_c.

$$\frac{4\pi R^3\rho_W g}{3} - \frac{16\pi R^2}{3}\frac{dT}{dz}\frac{d\sigma}{dT} + \frac{AR^2\sin^2\beta}{6d^3} = \frac{4\pi R^3\rho_B g}{3} + 2\pi\sigma R\sin^2\beta \tag{22}$$

As shown in Fig. 1(c), considering further that there is an angle between the freezing front and the horizontal plane α. Eq. (22) can be expressed as

$$\frac{4\pi R^3\rho_W g}{3} - \left(\frac{16\pi R^2}{3}\frac{dT}{dz}\frac{d\sigma}{dT} - \frac{AR^2\sin^2\beta}{6d^3}\right)\cos\alpha = \frac{4\pi R^3\rho_B g}{3} + 2\pi\sigma R\sin^2\beta\cos\alpha \tag{23}$$

Therefore, the air bubble detaching radius R_c can be expressed as

$$R_c = \frac{\left[\frac{3\sigma\sin^2\beta\cos\alpha(\rho_W-\rho_B)g}{2} + \cos^2\alpha\left(2\frac{dT}{dz}\frac{d\sigma}{dT} - \frac{A\sin^2\beta}{16\pi d^3}\right)^2\right]^{\frac{1}{2}} + \cos\alpha\left(2\frac{dT}{dz}\frac{d\sigma}{dT} - \frac{A\sin^2\beta}{16\pi d^3}\right)}{(\rho_W-\rho_B)g} \tag{24}$$

Consider that in extreme environments such as space, the gravity acceleration may be zero. Both buoyant force and gravity acting on the air bubble will disappear. Then the Eq. (25) can be expressed as

$$R_c = \frac{12\pi\sigma d^3\sin^2\beta}{A\sin^2\beta - 32\pi d^3\frac{dT}{dz}\frac{d\sigma}{dT}} \tag{25}$$

The temperature gradient around the air bubble at the freezing front is an important variable that affects the radius of the air bubble detachment. As shown in Fig. 4(a), the closer to the freezing front, the larger the temperature gradient. The temperature profile in the water is expressed as

$$T_w(t,z) = T_0 + (T_0 - T_{cp})\frac{1 - erf\left(\frac{z}{2\sqrt{\alpha_w t}}\right)}{1 - erf\left(C\sqrt{\frac{\alpha_i}{\alpha_w}}\right)} \tag{26}$$

where T_0 and T_{cp} are the water and cold plate temperatures at the initial moment, erf is the error function, C is a constant number related to the freezing front, and α_i and α_w are the thermal diffusivities of ice and water. The temperature gradient dT/dz in the water near the freezing front is expressed as

$$\frac{dT}{dz} = \frac{T_w(t,z+\Delta z) - T_w(t,z)}{\Delta z} \tag{27}$$

However, Eq. (25) is only suitable for calculating the temperature distribution in front of the freezing front, and is not suitable for calculating the temperature distribution around the air bubble due to the large thermal resistance of the bubble. To obtain the exact temperature gradient near the air bubble, the method of numerical simulation is used to calculate. To ensure the accuracy of the numerical simulation, Eq. (27) is used to test the temperature gradient in front of the freezing front. A cloud picture of the temperature distribution around the air bubble is shown in Fig. 4(b). From Eq. (27), It can be calculated that the temperature of point B at 50 μm from the freezing front is about 1.3 °C, which is 15% lower than the 1.5 °C obtained by numerical simulation, indicating high accuracy of numerical simulation results. The temperature at the bubble is 2.0 °C, and the temperature gradient there is 40,000 K/m. The detailed parameters for calculating the temperature gradient are listed in Table 1.

2.2. Experimental methodology

To observe the behavioral properties of air bubbles during the icing process, an experimental setup is constructed as shown in Fig. 5. The whole experimental setup consists of four parts, a control unit, a freezing unit, a data acquisition unit, and an auxiliary unit. The control unit consists of a thermostat, a power supply, a cooler, a heat exchanger, and a constant temperature bath. The freezing unit consists of a copper plate, and a Hele-Shaw cell consisting of two acrylic sheets. The data

Table 1
Parameters used to calculate the temperature gradient.

No.	Item	Parameter	Unit
1	C	0.202	/
2	T_0	25	°C
3	T_{cp}	−35	°C
4	z	1	mm
5	Δz	50	μm
6	α_i	1.17×10^{-6}	m^2/s
7	α_w	1.37×10^{-7}	m^2/s

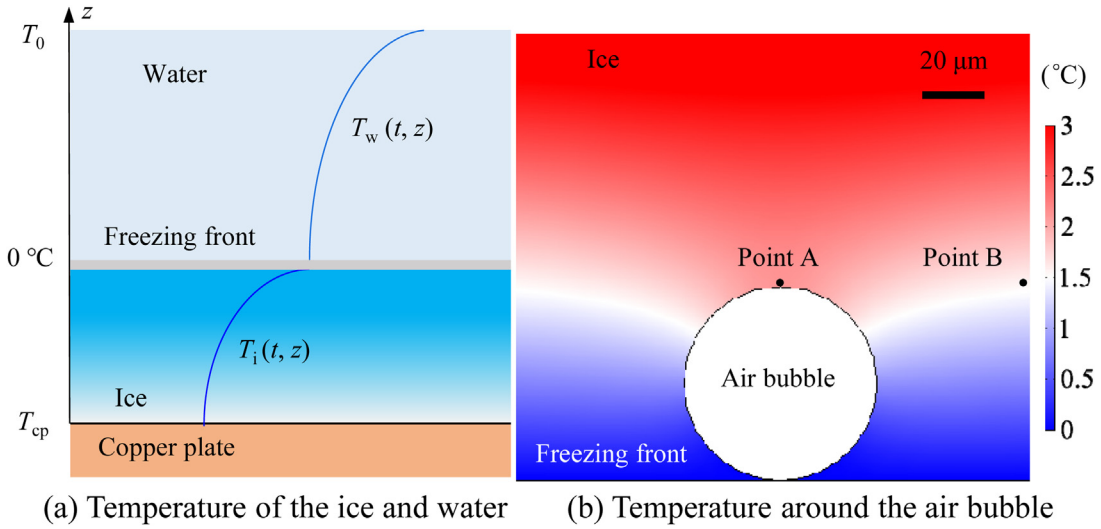

Fig. 4. Temperature distribution in water and ice during freezing.

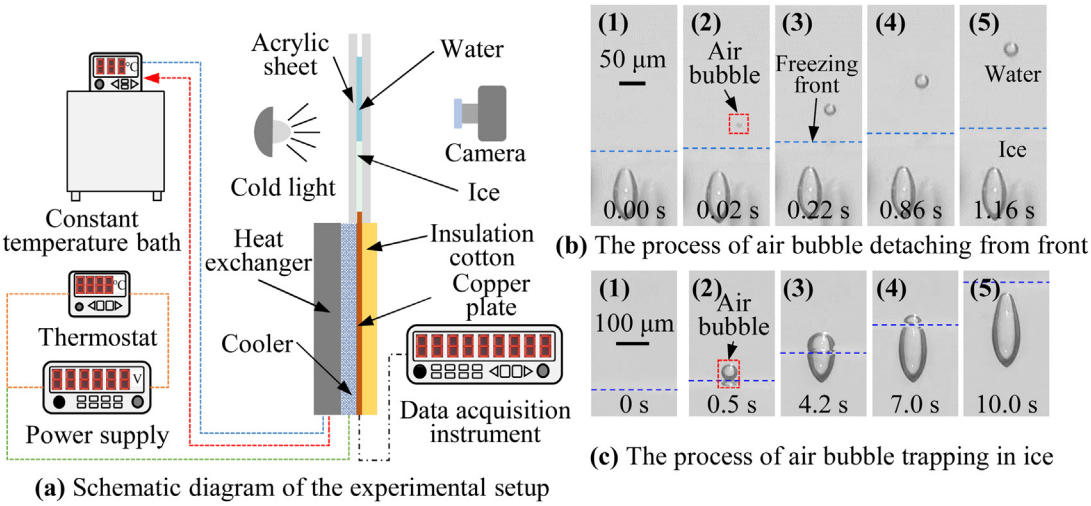

Fig. 5. Schematic of the experimental setup and the bubble behavior on freezing fronts.

Table 2
Descriptions of the experimental equipment used in this study.

Item	Equipment	Brand	Parameter
1	Camera	Canon	Frame frequency: 50 fps
2	Cold light	Luogen	Power: 35 W
3	Cooler	Ferrotec	Power: 80 W
4	Constant temperature bath	TENLIN	Accuracy: 0.2 °C
5	Date acquisition instrument	Agilent	Frequency: 2 Hz
6	Digital thermostat	OMRON	Accuracy: 1 °C
7	Power supply	MRINS	Accuracy: 0.01 V

acquisition unit consists of a data acquisition instrument that records real-time freezing temperatures and a camera that records air bubble morphology. A cold light, brackets for fixing line pipes, and equipment constitute the auxiliary unit. The detailed parameters of the equipment used in the experimental setup are listed in Table 2.

The Hele-Shaw cell is filled with 0.3 mm thick, 20 mm high saturated deionized water before the start of the experiment and then left to stand for 15 min. At the beginning of the experiment, the camera and data acquisition instrument are switched on first, then the cryostat and digital thermostat are switched on, and the film freezing experiment is carried out at a freezing temperature of −35 °C. The experimental results are shown in Fig. 5(b) and (c). The air bubbles on the freezing front exist in two states, detaching from the freezing front and being trapped in the ice (Video-2). To obtain the critical conditions for the air bubble to detach from the freezing front, a mathematical model is established to analyze the force of the air bubble on the freezing front during the icing process.

2.3. Validation of model

To verify the accuracy of the mathematical model developed in this study from the point of view of force equilibrium, the calculated values of the model are compared with the experimental values, and the results are displayed in Fig. 6. It can be seen that the calculated and experimental values of this model are in good agreement. The average error between the model-calculated air bubble detachment radius and the experimental values is < 35%. In addition, this model also has a higher accuracy than the other two mathematical models describing the radius of air bubble detachment. The accuracy of the Cole model is higher than that of the Maeno model [27]. The main reason for this phenomenon is

Table 3
Comparison of three models for predicting air bubble detachment radius.

Item	Schematic	Equation
Cole	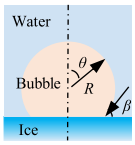	$\frac{\pi R^2 f(\theta)}{3}\left(\rho_W g R - 2\frac{dT}{dz}\frac{\partial\sigma}{\partial T}\right) = 2\pi R\sigma\sin^2\theta + \frac{\pi R^3 \rho_W g f(\theta)}{3} + \frac{2\pi R^2 f(\theta)}{3}\frac{dT}{dz}\frac{\partial\sigma}{\partial T}$ $f(\theta) = 2 + 3\cos\theta - \cos^3\theta$
Meano	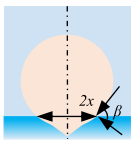	$V(\rho_W - \rho_B)g = 2\pi x\sigma\sin\theta$
This	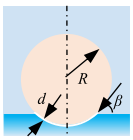	$\frac{4\pi R^3\rho_W g}{3} - \frac{16\pi R^2}{3}\frac{dT}{dz}\frac{d\sigma}{dT} + \frac{AR^2\sin^2\beta}{6d^3} = \frac{4\pi R^3\rho_B g}{3} + 2\pi\sigma R\sin^2\beta$

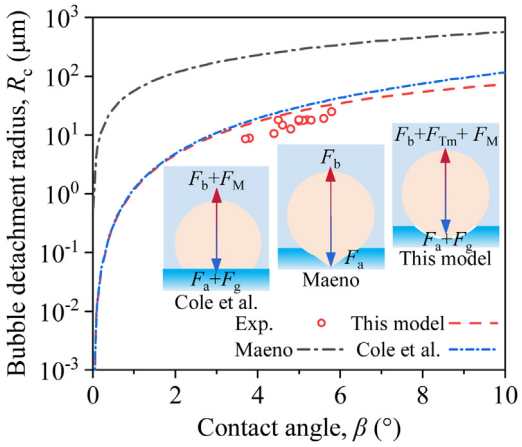

Fig. 6. Comparison of models for prediction of air bubble detachment radius.

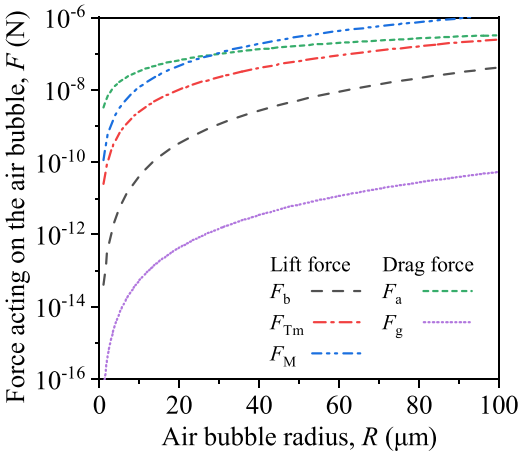

Fig. 7. Comparison of the magnitude of forces acting on air bubbles.

that these three mathematical models consider different forces acting on the air bubble. Cole's model assumes that the lift forces driving air bubbles away from freezing fronts are buoyant and Marangoni forces, while the drag forces are adhesion force and gravity. Maeno's model assumes that the lift forces are only buoyant forces and the drag forces are also only adhesion forces. This model analysis shows that the lift force includes buoyant force, thermomolecular force, and Marangoni force, and the drag force includes adhesion force and gravity. Since Maeno's model only considers buoyant as the lift force driving the air bubble to detach, its predicted radius of air bubble detachment is much larger than the experimental value. Compared with the Cole model, this model also considers thermomolecular forces due to the Gibbs-Thomson effect, causing its predictions to be closer to the experimental values.

To further compare the differences between the three models, both their model schematics and equations are listed in Table 3. From the table, it can be seen that the Cole model considers the contact surface of the air bubble and the freezing front to be a planar surface, and the part of the bubble in the water remains as a spherical portion during the growth process. The Meano model considers the contact portion of the air bubble and the freezing front to be a concave structure, and the shape of the bubble in the water is maintained as an ellipsoidal shape. The present model considers the air bubble on the freezing front to be spherical and there is a water film between the air bubble and the freezing front. As can be seen from the comparison of the predicted and experimental values of the three models in Fig. 6, the predictions of the present model are closer to the experimental values. Although the Cole model is also closer to the experimental values, compared with the present model, the Cole model only takes into account the buoyant force of the water on the air bubbles and the Marangoni force but not the force of the freezing front on the air bubbles. Moreover, the Cole model considers the shape of the air bubble over the freezing front to be part of a sphere, which will reduce the buoyant force on the air bubble.

To compare the relative magnitudes of the five forces acting on the air bubbles in this model, they are calculated as a function of the air bubble radius, and the relevant results are displayed in Fig. 7. All five forces gradually increase as the air bubble radius increases, but they do not increase to the same degree. When the air bubble radius is increased from 20 μm to 100 μm, the buoyant force and gravity all increase by a factor of 124 times, while the thermomolecular, temperature gradient and adhesion forces increase by a factor of 24 times, 24 times, and 4 times, respectively. This is because buoyant force and gravity are both proportional to the 3rd power of the air bubble radius, thermomolecular and Marangoni forces are proportional to the 2nd power of the radius, and adhesion force is proportional to only the 1st power of the radius. In ad-

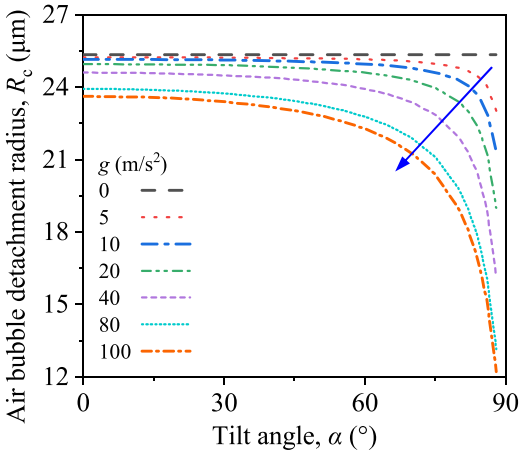

Fig. 8. Effect of tilt angle on air bubble detachment radius.

dition, adhesion forces, Marangoni forces, and thermomolecular forces are the three most important factors affecting the state of air bubbles in this condition, while buoyant force and gravity have less influence. Therefore, by changing the main factors affecting the state of air bubbles, it will be possible to directly control the detachment and trapping states of air bubbles.

3. Results and discussion

3.1. Effect of tilt angle on the air bubble

To investigate the factors affecting the state of air bubbles on the freezing fronts, the effects of different tilt angles between freezing fronts and the horizontal direction on the detachment radius of air bubbles and the forces acting on them at different gravitational accelerations are investigated, and the results are displayed in Fig. 8. It can be seen that the air bubble detachment radius does not change with the change of the tilt angle for the gravitational acceleration of 0 m/s^2. This is because the only forces acting on the air bubble are the thermomolecular force, the Marangoni force, and the adhesion force, which has nothing to do with the tilt angle between the freezing front and the horizontal direction. When the gravitational acceleration is greater than 0 m/s^2, the air bubble detachment radius tends to decrease with the increase of the angle. As the tilt angle increases, the proportion of thermomolecular force, Marangoni force, and adhesion force decreases, while the proportion of buoyant force and gravity force increases. This results in an increase in the lift force and a decrease in the drag force. As a result, the air bubble detachment radius tends to decrease gradually. In addition, the critical angle at which the air bubble detachment radius starts to decrease tends to decrease as the gravitational acceleration increases.

The effect of the tilt angle on the force acting on the air bubble at different gravitational accelerations is shown in Fig. 9. The buoyant force

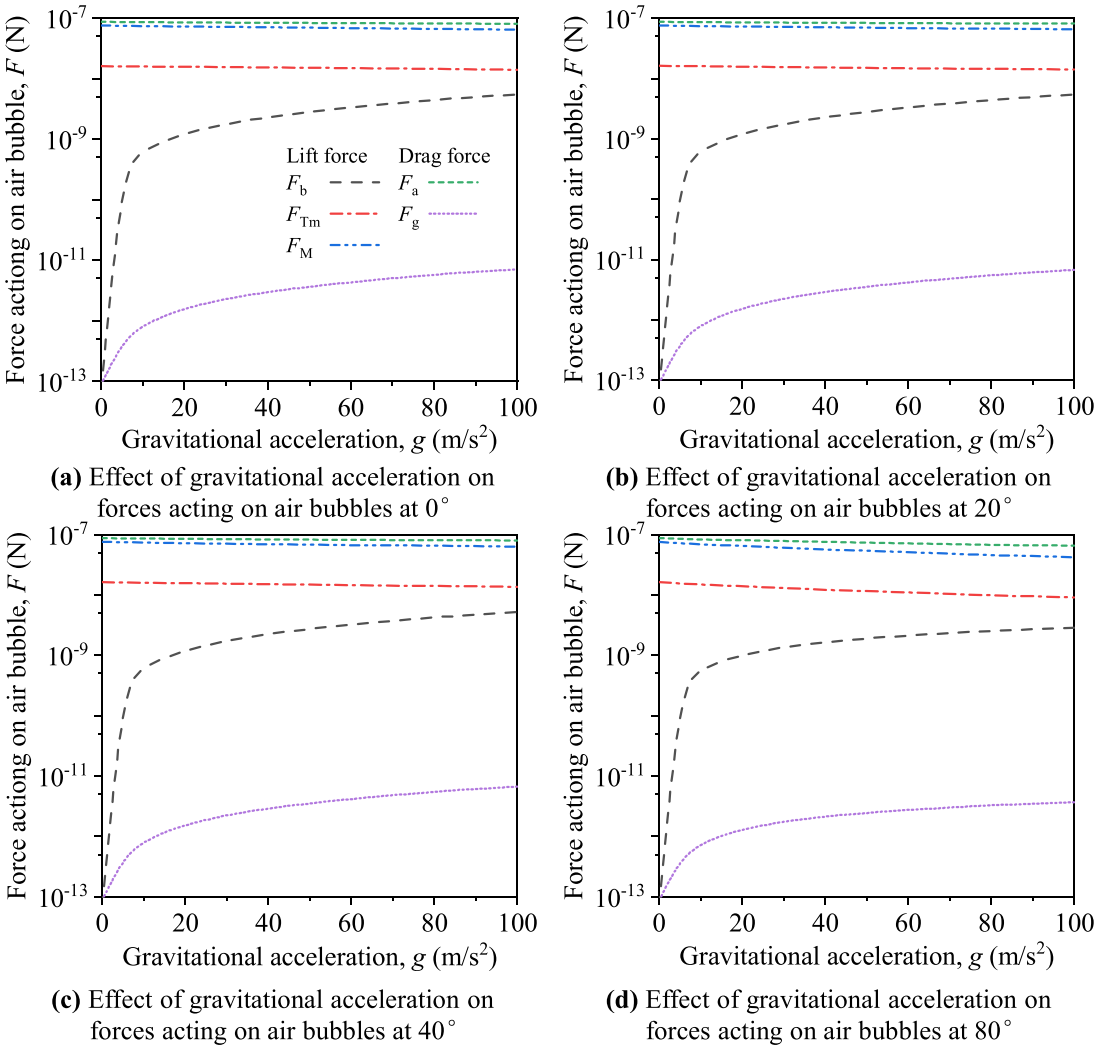

(a) Effect of gravitational acceleration on forces acting on air bubbles at 0°

(b) Effect of gravitational acceleration on forces acting on air bubbles at 20°

(c) Effect of gravitational acceleration on forces acting on air bubbles at 40°

(d) Effect of gravitational acceleration on forces acting on air bubbles at 80°

Fig. 9. Effect of tilt angle on forces acting on the air bubble.

and gravity gradually increase with the increase of gravitational acceleration at four different tilt angles, while the thermomolecular, Marangoni and adhesion forces show a decreasing trend. As the tilt angle increases, the degree of increase in buoyant force and gravity tends to decrease while the degree of decrease in the other three forces tends to increase. This is because buoyant force increases significantly with the gravitational acceleration, which leads to a gradual increase in the lift force. The increase in lift leads to a decrease in the growth time of air bubbles on the freezing front, which in turn leads to a decrease in their radius. The decrease in radius leads to a decrease in thermomolecular, Marangoni, and adhesion forces. As the tilt angle increases, the buoyant force becomes a progressively larger part of the combined force and the extent to which the air bubble detaches from the reduced radius increases.

The decrease in air bubble detachment radius with increasing gravitational acceleration for the same tilt angle may be caused by changes in buoyant force. When the gravitational acceleration increases, the buoyant force then increases linearly, resulting in a shorter growth time of the air bubbles at the freezing front, and thus a decrease in the detachment radius. This can also be verified by the fact that the change in buoyant force is the largest with increasing gravitational acceleration in Fig. 9. The decrease in the air bubble detachment radius with increasing tilt angle for the same gravitational acceleration is due to the decrease in the adhesion force. The component of the adhesion force in the vertical direction is proportional to the value of the cosine of the tilt angle. As the tilt angle increases, the component of the adhesion force decreases, resulting in a decrease in the air bubble detachment radius.

3.2. Effect of temperature gradient on the air bubble

A comparison of the relative magnitudes of the forces acting on air bubbles in Fig. 7 reveals that the Marangoni force is a major factor influencing the detachment of air bubbles from freezing fronts. Therefore, changing the temperature gradient of the water in front of the freezing front, which directly affects the Marangoni force, will significantly change the state of the air bubbles. The variation of the detachment radius of air bubbles with temperature gradient for different gravitational accelerations is demonstrated in Fig. 10. The air bubble detachment radius decreases with increasing gravitational acceleration at the same temperature gradient. At a temperature gradient of 1000 K/m, the air bubble detachment radius decreases from 124.2 μm to 63.4 μm when the gravitational acceleration increases from 0 to 100 m/s^2. The increase in gravitational acceleration leads to an increase in buoyancy, which results in a shorter growth time for the air bubble, leading to a decrease in its detachment radius. With the increase of temperature gradient, the air bubble detachment radius under different gravitational accelerations decreases gradually. Additionally, the difference in the gradual radius of the air bubble detachment at different gravitational accelerations gradually decreases and eventually tends to be equal. As the gravitational acceleration increases from 0 to 100 m/s^2, the air bubble detachment radius decreases from 135.5 μm to 65.3 μm for a 10 K/m temperature gradient, while the radius decreases from 13.2 μm and 12.9 μm for a 100,000 K/m temperature gradient. An increase in the temperature gradient leads to an increase in the lift force acting on the air bubble and a decrease in the radius of detachment of the air bubble. On the other hand, it also leads to an increase in the proportion of the Marangoni force in the lifting force, and the Marangoni force becomes the main factor affecting the detachment of air bubbles.

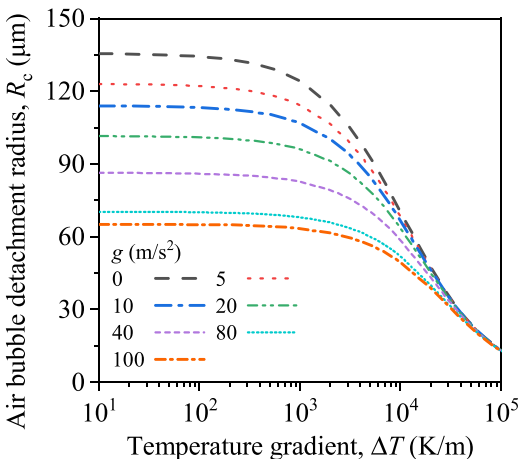

Fig. 10. Effect of temperature gradient on air bubble detachment radius.

The relative magnitudes of the five forces acting on the air bubble at four different temperature gradients are given in Fig. 11. Thermomolecular forces, Marangoni forces, and adhesion forces decrease gradually with increasing gravitational acceleration at different temperature gradients, while buoyant forces and gravity show opposite trends. All five forces show a gradual decrease with increasing temperature gradient. At a temperature gradient of 10 K/m, when gravitational acceleration increases from 0 m/s^2 to 100 m/s^2, the buoyant force, thermomolecular force, Marangoni force, adhesion force, and gravity force change from 0 N, 4.65×10^{-7} N, 4.31×10^{-10} N, 4.65×10^{-7} N, 0 N to 1.16×10^{-7} N, 1.08×10^{-7} N, 9.99×10^{-11} N, 2.24×10^{-7} N, 1.50×10^{-10} N. The buoyant, thermomolecular, temperature gradient, adhesion, and gravity forces change from 0 N, 4.43×10^{-9} N, 4.10×10^{-8} N, 4.54×10^{-8} N, 0 N to 9.08×10^{-10} N, 4.25×10^{-9} N, 3.93×10^{-8} N, 4.48×10^{-7} N, 1.17×10^{-12} N when the acceleration of gravity is increased from 0 m/s^2 to 100 m/s^2 at a temperature gradient of 100,000 K/m. At a gravitational acceleration of 0 m/s^2, the proportion of the Marangoni force in the lift force changes from 0.09% to 0.04% as the temperature gradient increases from 10 K/m to 100,000 K/m. At a gravitational acceleration of 100 m/s^2, the proportion of the Marangoni force in the lift force changes from 90.25% to 88.40% as the temperature gradient increases from 10 K/m to 100,000 K/m. For the same temperature gradient, the proportion of the Marangoni force of the lift force decreases with increasing gravitational acceleration. For the same gravitational acceleration, the proportion of the Marangoni force in the lift force becomes larger with increasing temperature gradient.

As the temperature gradient increases, the air bubble detachment radii at different gravitational accelerations all eventually converge to the same. This is because the Marangoni force increases as the temperature gradient increases. When the temperature gradient is greater than 10,000 K/m, the Marangoni force dominates the lift force. As the temperature gradient increases further, the proportion of Marangoni force gradually increases, and the effects of buoyant and thermomolecular forces are gradually weakened or even can be neglected. At this time, it is mainly the Marangoni force and the adhesion force that affect the air bubble detachment radius. The gravitational acceleration only affects the buoyant force and gravity, but not the Marangoni force. In addition, only the buoyant force and gravity increase rapidly with the increase of gravitational acceleration. The gradual decrease of Marangoni force and thermomolecular force is caused by the increase of buoyant force resulting in the decrease of the air bubble detachment radius.

3.3. Effect of liquid density on the air bubble

The effect of gravitational acceleration on the detachment radius of an air bubble and the force acting on it for different liquid densities is shown in Fig. 12. When the acceleration of gravity is 0, the buoyant force acting on the bubble is also 0, and thus the liquid density in this condition does not affect the air bubble detachment radius. In other working conditions, the detachment radius shows a gradual decrease with the increase of both liquid density and gravitational acceleration.

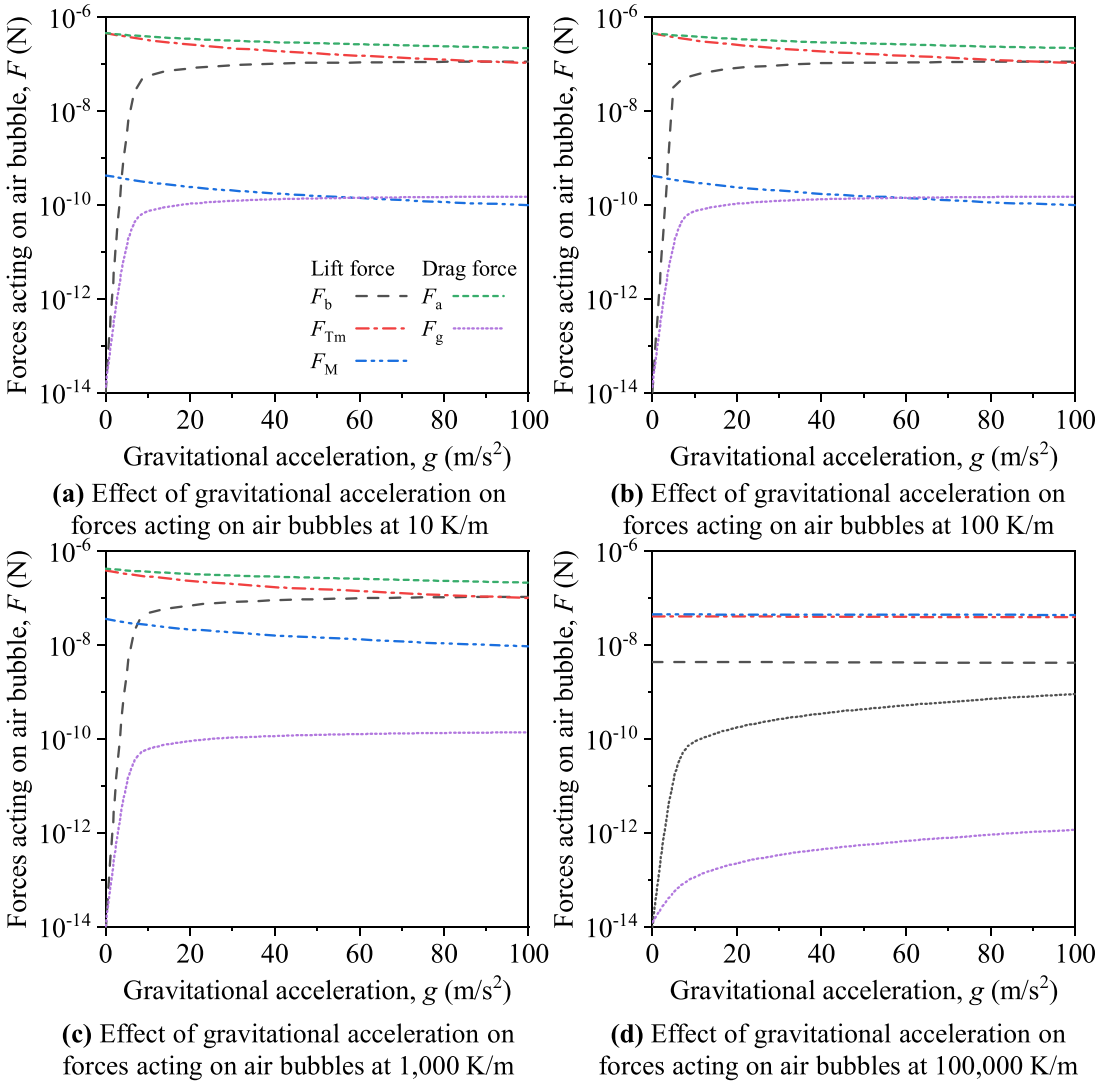

Fig. 11. Effect of temperature gradient on forces acting on the air bubble.

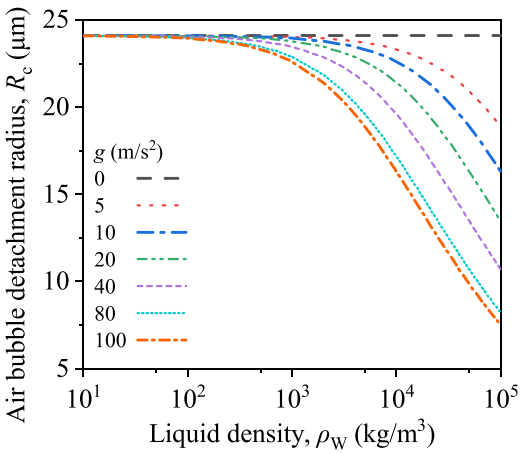

Fig. 12. Effect of liquid density on air bubble detachment radius.

Additionally, the difference between the air bubble detachment radii at each gravitational acceleration gradually increases as the density of the liquid increases. At a liquid density of 10 kg/m^3, the air bubble detachment radius almost changes as the gravitational acceleration increases from 0 m/s^2 to 100 m/s^2. At a liquid density of 100,000 kg/m^3, the air bubble detachment radius gradually decreases from 24.1 μm to 7.5 μm as the gravitational acceleration increases from 0 m/s^2 to 100 m/s^2. This is because the buoyant force gradually increases as the gravitational acceleration and the liquid density increase. This increase in buoyant force will result in a decrease in the radius of detachment of the air bubble.

Centrifugal casting is a commonly used metal smelting method, in the centrifugal force under the action of the liquid metal can be well filled with casting, while the centrifugal force also helps to liquid metal in the gas and inclusions in the exclusion of the casting, so as to improve the casting of mechanical properties and physical properties. The density of different metals has a large difference, when the metal density of 1000 kg/m^3, with the increase of gravitational acceleration, the bubble detachment radius gradually decreases. As the gravitational acceleration increases from 10 m/s^2 to 80 m/s^2, the air bubble detachment radius decreases from 23.9 μm to 23.8 μm, 23.5 μm, and 22.8 μm, with decreases of 0.67%, 1.30%, and 2.47%. At a metal density of 10,000 kg/m^3, the radius decreases from 22.6 μm to 21.4 μm, 19.6 μm and 17.2 μm, with decreases of 5.27%, 8.46% and 12.35%. It shows that the effect of gravitational acceleration on the air bubbles at the solidification interface of the metal increases with its density. This suggests that removing air bubbles of the same size during metal casting requires a low gravitational acceleration for denser metals.

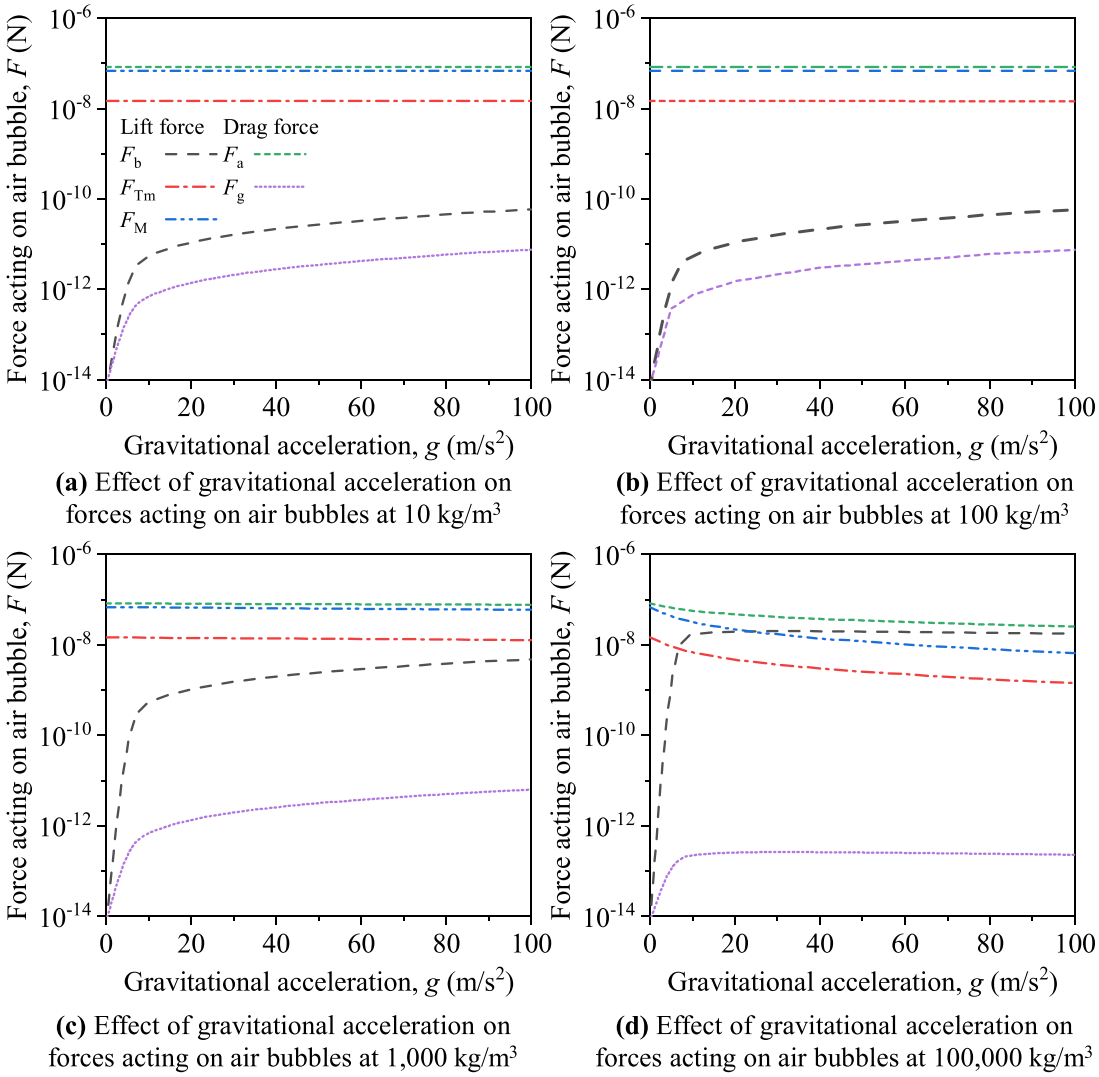

Fig. 13. Effect of liquid density on forces acting on the air bubble.

To further investigate the effect of liquid density on the air bubble detachment radius, the trends of the five forces acting on air bubbles with gravitational acceleration are studied for four different liquid densities, and the results are shown in Fig. 13. In two liquids with densities of 10 kg/m^3 and 1000 kg/m^3, with increasing gravitational acceleration, the buoyant force and gravity tend to increase, while the thermomolecular, Marangoni and adhesion forces tend to decrease. In liquids density of 100,000 kg/m^3, with the increasing gravitational acceleration, the buoyant force and gravity tend to increase and then decrease while the thermomolecular, Marangoni, and adhesion forces tend to decrease. This is because as the liquid density increases, the buoyant force increases, resulting in a decrease in the radius. As the liquid density increases further, the buoyant force decreases as the radius decreases more than the increase in buoyant force brought about by the increase in liquid density.

The air bubble detachment radius decreases as the liquid density and the gravitational acceleration increase. This is because the buoyant force is proportional to both the liquid density and the gravitational acceleration. The increase in buoyant force increases the lift force, which in turn leads to a decreased air bubble detachment radius. When the liquid density is greater than 1000 kg/m^3, the radius starts to decrease rapidly. This is because the buoyant force starts to dominate in the lift force, which can also be seen in Fig. 13, when the liquid density is greater than 10,000 kg/m^3, the buoyant force is comparable to the adhesion force. This leads to a gradual decrease in the air bubble detachment radius as the liquid density and gravitational acceleration increase.

4. Discussion

To investigate the effect of different factors on the air bubble detachment radius under different gravitational accelerations, the tilt angle, temperature gradient, and liquid density on the detachment radius are compared, and the results are displayed in Fig. 14. As the gravitational acceleration increases, the air bubble detachment radius all decreases. As the tilt angle increases, the decrease in the air bubble detachment radius becomes larger with the increase in gravitational acceleration. When the gravitational acceleration increases from 0 m/s^2 to 100 m/s^2, the air bubble detachment radius decreases by 10.84%, 11.17%, 12.38%, 15.53%, and 27.45% at five different tilt angles. The air bubble detachment radius decreases by 51.83%, 51.56%, 48.92%, 29.77%, and 2.04% at five different temperature gradients. The air bubble detachment radius decreases by 0.07%, 0.70%, 6.22%, 32.37%, and 68.82% at five different liquid densities. Increasing the tilt angle reduces the air bubble detachment radius, but the change is small. Increasing the temperature gradient also reduces the detachment radius, but to a lesser extent as the gravitational acceleration increases. As the liquid density increases, the detachment radius decreases, but to a greater extent with increasing gravitational acceleration.

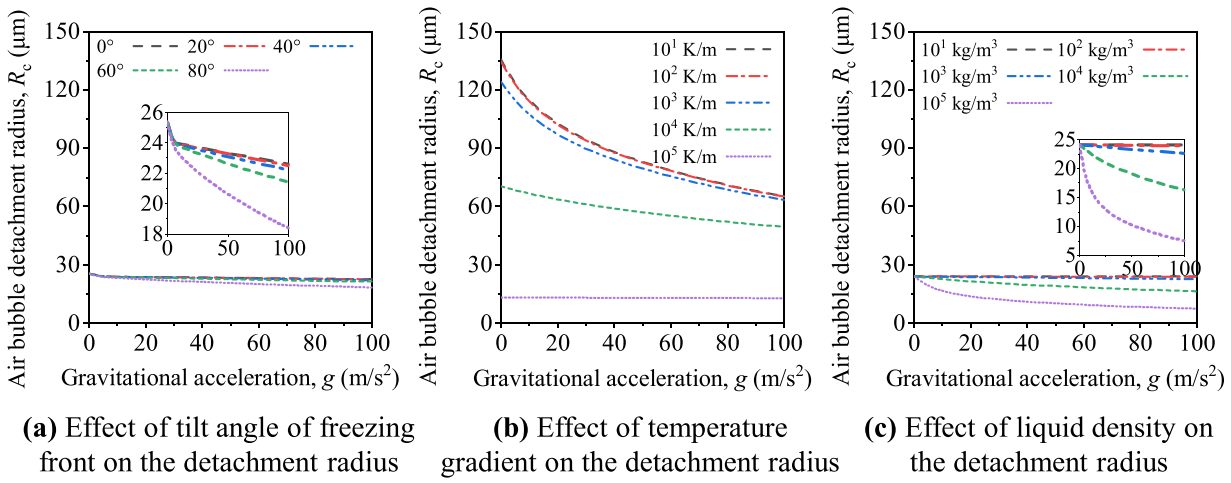

(a) Effect of tilt angle of freezing front on the detachment radius

(b) Effect of temperature gradient on the detachment radius

(c) Effect of liquid density on the detachment radius

Fig. 14. Effect of different factors on the air bubble detachment radius.

To make the results more general, a non-dimensional calculation of the detachment radius of the bubbles is performed. The above study shows that the gravity of the air bubble is much less than the other forces, so it is ignored to simplify the calculations. Then Eq. (22) can be expressed as

$$\frac{4\pi R^2\rho_W g}{3\sigma}-\frac{16\pi R}{3\sigma}\frac{dT}{dz}\frac{d\sigma}{dT}+\frac{A R\sin^2\beta}{6d^3\sigma}=2\pi\sin^2\beta \tag{28}$$

$$8\pi d^3\sigma Bo+\left(A\sin^2\beta-32\pi d^3\frac{dT}{dz}\frac{d\sigma}{dT}\right)R=12d^3\sigma\pi\sin^2\beta \tag{29}$$

$$R=\left(12d^3\sigma\pi\sin^2\beta-8\pi d^3\sigma Bo\right)/\left(A\sin^2\beta-32\pi d^3\frac{dT}{dz}\frac{d\sigma}{dT}\right) \tag{30}$$

From the relationship between the detachment radius of air bubbles and the dimensionless Bond number shown in Fig. 15, it can be seen that the radius decreases as the Bond number increases. When the Bond number is $< 10^{-6}$, the radius decreases more drastically. This shows that the buoyant force as a percentage of all forces on the bubble increases gradually with the Bond number. For pure water, an increase in Bond number indicates an increase in gravitational acceleration. It also indicates that the effect of gravitational acceleration on the radius of air bubble detachment increases gradually with its increase.

To investigate the effect of air bubbles in ice on the physical properties of ice, numerical simulations are used to investigate the effect of air bubbles on the mechanical and thermal properties of ice, the parameters of the numerical simulation are shown in Table 4. As shown in Fig. 16(a) and (b), the stress distributions on bubble ice and clear ice under the same force are demonstrated. Under the same external force, the maximum stress in the air bubble ice is 2.5 MPa, while that in the clear ice is only 0.6 MPa. The stress on the clear ice is uniformly distributed, while the stress around the air bubbles in the air bubble ice is

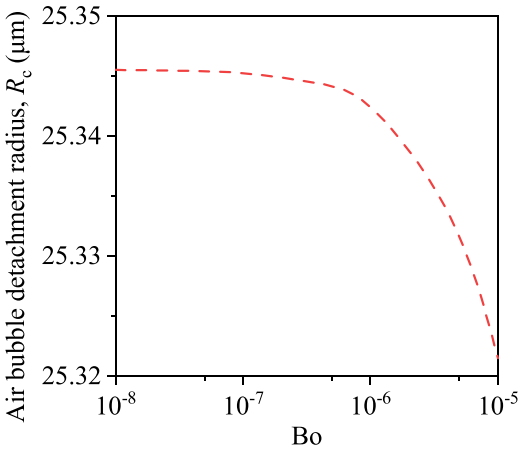

Fig. 15. Variation of air bubble detachment radius with Bond number.

obviously higher than in the other locations. This indicates that the bubble will become a stress concentration area under external force, and the compressive strength of bubble ice is lower than that of clear ice. The effect of bubbles on the thermal properties of ice is shown in Fig. 16(c) and (d), where bubble ice of the same volume is somewhat hotter than clear ice for the same heat flux. The maximum and minimum temperatures of bubble ice are −10 °C and −18.8 °C, while those of clear ice are −15.5 °C and −19.8 °C. For the same volume, bubble ice has less mass than clear ice, and thus its heat transfer rate is faster. When heat is used to remove ice from the surface of the substrate, due to the greater thermal resistance of the bubbles in the ice, the area where the bubbly ice comes into contact with the substrate heats up faster under the same

Table 4
Parameters for numerical simulation.

No.	Item	Parameter	Unit
1	Size	Ice: 200 × 160, Bubble: 160 × 100	mm
2	Young's modulus	5.5	GPa
3	Poisson's ratio	0.3	/
4	Load	50,000	N/m^2
5	Density	920	kg/m^3
6	Thermal conductivity	2.2	W/(m·K)
7	Initial temperature	−20	°C
8	Heat flux	200	W/m^2

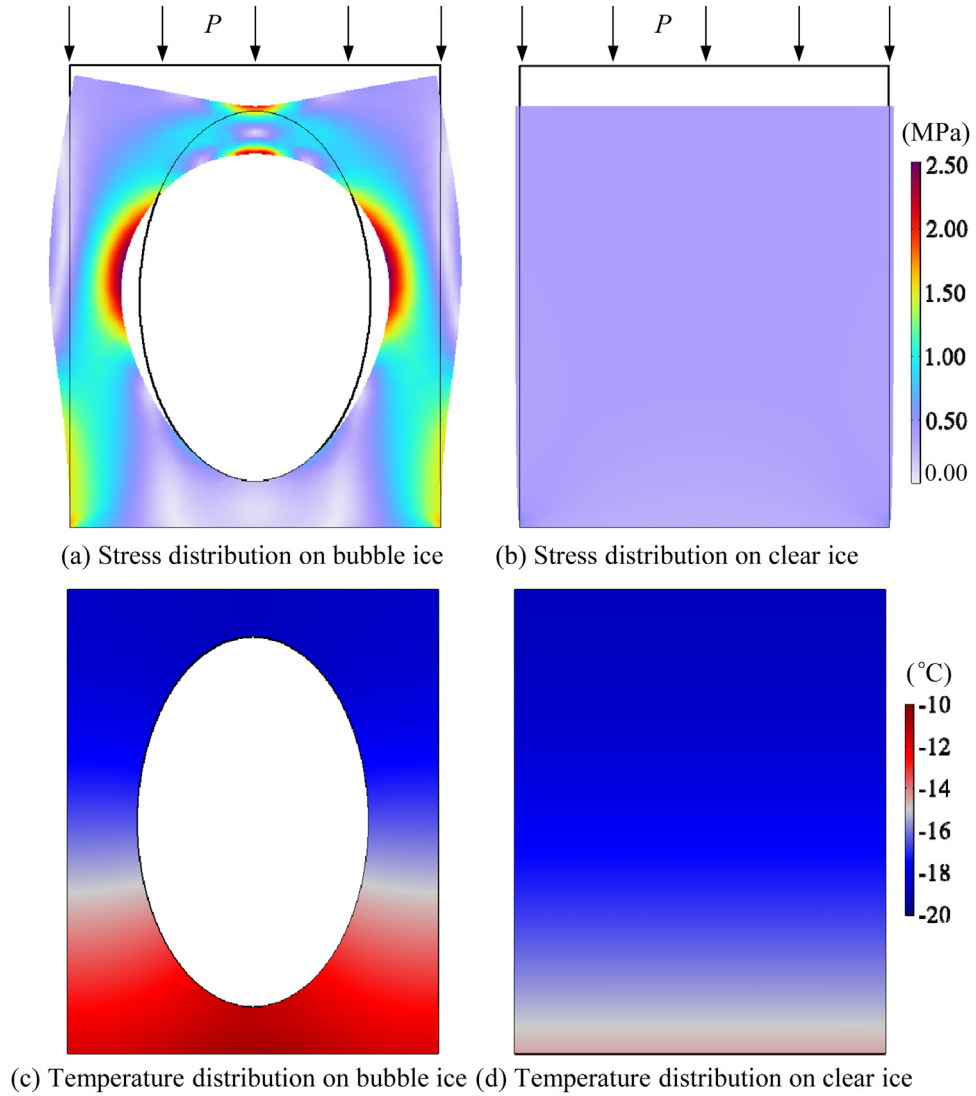

Fig. 16. Effect of air bubbles on the mechanical and thermal properties of ice.

conditions, which will also reduce energy consumption and increase the efficiency of de-icing.

5. Conclusion

To obtain the critical conditions for the detachment and trapping of tiny air bubbles on freezing fronts under different gravitational accelerations, a mathematical model is developed and validated based on the principle of equilibrium of forces acting on air bubbles. Based on this model, the critical conditions affecting the detachment of air bubbles are investigated, and the following conclusions are acquired.

(1) The air bubble detachment radius at different gravitational accelerations tends to decrease as the tilt angle increases. This decreasing trend becomes larger with increasing gravitational acceleration. The air bubble detachment radius at different gravitational accelerations decreases with increasing temperature gradient. This decreasing trend becomes smaller with increasing gravitational acceleration, and the air bubble detachment radius tends to be the same for all cases.

(2) The air bubble detachment radius at different gravitational accelerations tends to decrease as the liquid density increases. This decreasing trend becomes larger as the gravitational acceleration increases. The air bubble detachment radius decreases with increasing gravitational acceleration, for different tilt angles, temperature gradients, and liquid densities. The decrease of air bubble detachment radius increases with the increase of gravitational acceleration for different tilt angles and liquid densities, while the decrease of air bubble detachment radius decreases with the increase of gravitational acceleration for different temperature gradients.

(3) Based on this model, the effects of the tilt angle of the freezing front, temperature gradient, and liquid density on the bubble detachment radius and the relative magnitude of the force acting on the bubbles in different gravitational environments are explored, and some patterns of change are derived. However, this model is limited to a single-factor analysis of the influencing factors, and the actual influence of the factors will also affect each other. When the tilt angle of the freezing front changes, the temperature gradient will also change. Therefore, the subsequent model can take the coupling influence of the factors into account, which can get a more accurate influence law.

Data availability

Data will be made available on request.

Declaration of competing interest

The authors declare that they have no conflicts of interest in this work.

Acknowledgments

This research is funded by the Beijing Municipal Commission of Science and Technology, Zhongguancun Science and Technology Park Management Committee (Z231100006123010, 3244046 and 3232032), Department of Science and Technology of Hebei Province (244A7625D), National Natural Science Foundation of China (52406007 and 52306003), Key Laboratory of Icing and Anti/Deicing (IADL20230113 and IADL20220304), Young Elite Scientist Sponsorship Program by BAST (BYESS2023352), and China Scholarship Council (202406030128).

Supplementary materials

Supplementary material associated with this article can be found, in the online version, at doi:10.1016/j.fmre.2025.03.014.

References

[1] T.Y. Wang, S.L. He, Q.H. Zhang, et al., Ice sheet expansion in the cretaceous greenhouse world, Fundamental Research 4 (6) (2024) 1586–1593.
[2] B. Ji, Z. Yang, J. Feng, Compound jetting from bubble bursting at an air-oil-water interface, Nat. Commun. 12 (2021) 6305.
[3] Y. Guo, Q.Q. Zhu, S.L. Song, et al., Bubble dynamics of flow boiling in microchannel within ultrasonic field, Int. Commun. Heat Mass. 159 (2024) 108180.
[4] K.K. Shao, M.J. Song, Z.Y. Jiang, et al., Experimental study on the formation and distribution of trapped air bubbles in horizontal ice slice (in Chinese), CIESC J 74 (S1) (2023) 161–164.
[5] H. Jamgotchian, R. Trivedi, B. Billia, Interface dynamic and couple growth in directional solidification in presence of bubbles, J. Cryst. Growth 134 (1993) 181–195.
[6] H.J. Cho, J.P. Mizerak, E.N. Wang, Turning bubbles on and off during boiling using charged surfactants, Nat. Commun. 6 (2015) 8599.
[7] H.Y. Zhan, Z.C. Yuan, Y. Li, et al., Versatile bubble maneuvering on photopyroelectric slippery surfaces, Nat. Commun. 14 (2023) 6158.
[8] A.T. Oratis, J.W.M. Bush, H.A. Stone, et al., A new wrinkle on liquid sheets: Turning the mechanism of viscous bubble collapse upside down, Science 369 (6504) (2020) 685–688.
[9] A.M. Zhang, S.M. Li, P. Cui, et al., A unified theory for bubble dynamics, Phys. Fluids 35 (3) (2023) 033323.
[10] K.K. Shao, M.J. Song, J. Shen, et al., Experimental study on the distribution and growth characteristics of trapped air bubbles in ice slices at different freezing temperatures, Appl. Therm. Eng. 244 (3) (2024) 122600.
[11] Q. Dang, M.J. Song, X. Zhang, et al., Experimental study about solidification processes of sessile deformed water droplets on the biaxial inclined cold plate surface under natural convection, Appl. Therm. Eng. 236 (2024) 121883.
[12] K. Matsumoto, K. Furuya, S.Y. Zhang, et al., Investigation on concentration characteristics of ozone micro-bubbles fixed in ice and ozone gas released from ice, Int. J. Refrig. 53 (2015) 13–19.
[13] X. Zhang, X. Liu, X.M. Wu, et al., Impacting-freezing dynamics of a supercooled water droplet on a cold surface: Rebound and adhesion, Int. J. Heat Mass Tran. 158 (2020) 119997.
[14] L. Stendardo, G. Gastaldo, M. Budinger, et al., Why the adhesion strength is not enough to assess ice adhesion on surfaces, Appl. Surf. Sci. 672 (2024) 160740.
[15] K.K. Shao, M.J. Song, X. Zhang, et al., A review of micro-scale trapped air bubble growth distribution characteristics and thermal mechanical effects in ice, J. Harbin Inst. Technol. 56 (6) (2024) 152–174 Chinese.
[16] K. Murakami, H. Nakajima, Formation of pores during unidirectional solidification of water containing carbon dioxide, Mater. Trans. 43 (2002) 2582–2588.
[17] K.K. Shao, M.J. Song, X. Zhang, et al., Growth and distribution characteristics of trapped air bubbles in ice slices, Phys. Fluids 35 (2023) 113319.
[18] N. Maeno, Air bubble formation in ice crystals, Phys. Snow Ice: proc. 1 (1) (1967) 207–218.
[19] A.E. Carte, Air bubble in ice, Proc. Phys. Soc. 77 (1961) 757–768.
[20] J.G. Meijer, D. Rocha, A.M. Linnenbank, et al., Enhanced bubble growth near an advancing solidification front, J. Fluid Mech. 996 (2024) A22.
[21] K.K. Shao, Z.J. Zhen, R.M. Gao, et al., Comparative experimental study of the effect of loading rate on the typical mechanical properties of bubble and clear ice cubes, Exp. Therm. Fluid Sci. 159 (2024) 111264.
[22] K.K. Shao, M.J. Song, B.H. Cai, et al., Effect of environmental temperature and trapped air bubbles on the mechanical properties of ice cubes, ACS Appl. Mater. Interfaces 16 (46) (2024) 63482–63494.
[23] H. Shi, M.J. Song, J.F. Ge, et al., A high-precision saltwater ice thickness and salinity detection method based on capacitive coupled planar microwave resonator, Cold Reg. Sci. Technol. 231 (2025) 104417.
[24] Y. Li, Are bubbles in ice the potential space for hydrogen storage, Int. J. Hydrogen Energ. 50 (2024) 575–585.
[25] R.M. Gao, M.J. Song, C.Y.H. Chao, et al., Review on condensation frosting and defrosting experiments for superhydrophobic surfaces, Appl. Therm. Eng. 236 (2024) 121693.
[26] K.H.S. Bagdasarov, V.V. Okinshevich, A. Kholov, On the theory of capture of gas bubbles by a crystal growing from the melt, Phys. Stat. Sol. 58 (1980) 317–322.
[27] R. Cole, J.M. Papazian, W.R. Wilcox, Bubble departure radii at solidification interfaces, Int. J. Heat Mass Transf. 23 (1980) 219–224.
[28] B.A. Lomax, G.H. Just, P.J. McHugh, et al., Predicting the efficiency of oxygen-evolving electrolysis on the moon and mars, Nat. Commun. 13 (2022) 583.
[29] C. Gabrielli, F. Huet, M. Keddam, et al., Potential drops due to an attached bubble on a gas-evolving electrode, J. Appl. Electrochem. 19 (1989) 617–629.
[30] K.F. Vasconcellos, J. Beech, The development of blowholes in the ice/water/carbon dioxide system, J. Crystal Growth 28 (1975) 85–92.
[31] K.K. Shao, M.J. Song, X. Zhang, et al., Mechanical analysis of the critical conditions for trapping and detachment of microscale air bubbles on the pure water freezing front, Langmuir 40 (47) (2024) 25334–25343.
[32] D.C. Guo, T. Dou, H. Zou, et al., Frost-preventing design for space station refrigerator, Energies 6 (2003) 7801.
[33] J.M. Papazoan, W.R. Wilcox, Interaction of bubbles with solidification interfaces, AIAA J 16 (5) (1978) 447–451.
[34] J.A. Sarabia-Alonso, J.G. Ortega-Mendoza, J.C. Ramírez-San-Juan, et al., Optothermal generation, trapping, and manipulation of microbubbles, Opt. Express 28 (12) (2020) 17672–17682.
[35] M.S. Park, A.A. Golovin, S.H. Davis, The encapsulation of particles and bubbles by an advancing solidification front, J. Fluid Mech. 560 (2006) 415–436.
[36] X.H. Zhang, H.Y. Sun, H. Zhao, et al., Formation and stabilization of CO_2 bubbles with different sizes and the interaction with solid particles, Colloid Surf. Physicochem. Eng. Asp. 598 (2020) 124815.
[37] J.S. Wettlaufer, M.G. Worster, L.A. Wilen, et al., A theory of premelting dynamics for all power law forces, Phys. Rev. Lett. 76 (19) (1996) 3602–3605.
[38] L.A. Wilen, J.S. Wettlaufer, M. Elbaum, et al., Dispersion-force effects in interfacial premelting of ice, Phys. Rev. B 52 (16) (1995) 12426–12433.
[39] B. Saint-Michel, M. Georgelin, S. Deville, et al., Internation of multiple particles with a solidification front: From compacted particle layer to particle trapping, Langmuir 33 (23) (2017) 5617–5627.
[40] A.W. Rempel, M.G. Worster, Particle trapping at an advancing solidification front with interfacial-curvature effects, J. Cryst. Growth 223 (2001) 420–432.

Author profile

Keke Shao is a Ph.D. candidate at the Beijing Institute of Technology and a visiting Ph.D. student in the University of Tokyo. He received his B.S. degree from Zhengzhou University, the M.S. degree from China University of Mining and Technology, Beijing. His current research mainly focuses on the icing mechanism and trapped air bubbles in ice.

Mengjie Song (BRID: 05300.00.33986) is a professor and doctoral supervisor at the School of Mechanical Engineering, Beijing Institute of Technology, and is recognized as a national-level high-caliber young talent. He received his B.S. degree from Hunan University, the M.S. degree from Harbin Institute of Technology, and his Ph.D. degree from The Hong Kong Polytechnic University. His research primarily focuses on the thermodynamic mechanisms and applied fundamental studies of complex fluid phase change. He has published 202 papers in these fields, including 130 as first author or corresponding author. Additionally, he has led 33 research projects, including the National Natural Science Foundation of China, the Ministry of Industry and Information Technology, and the Science and Technology Commission of the Central Military Commission.